QUANTUM GASES

Topological pumping of a 1D dipolar gas into strongly correlated prethermal states

Wil Kao[1,2]*, Kuan-Yu Li[1,2]*, Kuan-Yu Lin[2,3], Sarang Gopalakrishnan[4,5], Benjamin L. Lev[1,2,3]†

Long-lived excited states of interacting quantum systems that retain quantum correlations and evade thermalization are of great fundamental interest. We create nonthermal states in a bosonic one-dimensional (1D) quantum gas of dysprosium by stabilizing a super-Tonks-Girardeau gas against collapse and thermalization with repulsive long-range dipolar interactions. Stiffness and energy-per-particle measurements show that the system is dynamically stable regardless of contact interaction strength. This enables us to cycle contact interactions from weakly to strongly repulsive, then strongly attractive, and finally weakly attractive. We show that this cycle is an energy-space topological pump (caused by a quantum holonomy). Iterating this cycle offers an unexplored topological pumping method to create a hierarchy of increasingly excited prethermal states.

Highly excited eigenstates of interacting quantum systems are generically "thermal," in the sense that they obey the eigenstate thermalization hypothesis (*1*): Physical observables behave in these excited states as they would in thermal equilibrium. For generic thermal systems, all initial conditions give rise to locally thermal behavior at times past the intrinsic dynamical time scale. Systems in which thermalization is absent are of great fundamental interest because they violate equilibrium statistical mechanics, and of technological interest because some quantum information in these states evades decoherence. Nonthermal excited states exist in integrable (*2*, *3*) and many-body localized (*3*, *4*) systems. More recently, it has been realized that even nonintegrable systems might have special excited initial states for which thermalization is absent; these states are called quantum many-body scars (*5*–*10*). Both integrability and scars are fine-tuned, and can thus only be approximately realized in actual experiments, in the form of long-lived prethermal states. As anticipated in (*10*, *11*), approximate integrability can give rise to states that closely resemble scars: i.e., atypical initial states with unexpectedly long relaxation times. In such prethermal states, one would expect observables to remain far from their thermal value for long times. Much about the classification, physical origins, and lifetimes of such atypical initial states remains unclear.

In this work, we demonstrate a "topological" pumping protocol for creating a hierarchy of atypical prethermal states by cyclically varying the short-range (contact) interaction strength of a dipolar Bose gas confined in one dimension. The cycles are made possible through dipolar stabilization of the gas. In a conventional topological pump (*12*), the Hamiltonian returns to itself after one cycle, but the state is translated by one lattice site. In the present setup, by contrast, the state is translated up the many-body energy spectrum; thus, this protocol maps each eigenstate to an eigenstate with an extensively higher energy. This effect is called a "quantum holonomy" (*13*). A toy example that illustrates this effect is a particle subject to a δ-function potential. The nth even-parity eigenstate for an infinitely repulsive potential is identical to the $(n + 1)$th even-parity eigenstate for an infinitely attractive potential. Hence, by cycling the potential from zero to infinitely repulsive, to infinitely attractive and back to zero, one can wind up the phase of the wave function and create a sequence of increasingly excited states (*14*). Here, we show that dipolar interaction-stabilized approximate integrability allows one to implement a many-body version of this cycle without simply heating up the system. This many-body cycle enables one to generate nonthermal highly excited states with high fidelity.

The one-dimensional (1D) gas system forms an attractively interacting, excited "super-Tonks-Girardeau" gas (sTG) at an intermediate stage of the many-body holonomy cycle implemented here. The bosons in this state are even more strongly anticorrelated than free fermions (*15*–*20*). As one quenches deeper into the sTG regime by making the contact interactions less strongly attractive, one expects the sTG to become unstable; this is indeed seen in gases with purely short-range interactions (*18*). Unexpectedly, however, even though the dipole-dipole interaction (DDI) breaks integrability (*21*), it enhances the stability of the sTG regime (relative to the purely short-range case). This allows one to implement the entire cycle, thus realizing this previously unobserved topological pumping phenomenon. [Dipolar sTGs have been predicted to exist in contexts different from that realized here; see (*22*) for discussion.]

We implement the following protocol. First, we create a low-temperature dipolar 1D Bose gas in a regime with weak repulsive contact interactions. We then tune the scattering length across confinement-induced resonances (CIRs) of colliding atoms (*23*–*26*) in the following stages. First, we ramp up the contact interactions toward the resonance, so the gas adiabatically enters the strongly antibunched Tonks-Girardeau (TG) state (*27*–*29*). At this point, we quench these interactions across the resonance, from strongly repulsive to strongly

[1]Department of Applied Physics, Stanford University, Stanford, CA 94305, USA. [2]E. L. Ginzton Laboratory, Stanford University, Stanford, CA 94305, USA. [3]Department of Physics, Stanford University, Stanford, CA 94305, USA. [4]Physics and Astronomy, CUNY College of Staten Island, Staten Island, NY 10314, USA. [5]Physics Program and Initiative for Theoretical Sciences, The Graduate Center, CUNY, New York, NY 10016, USA.
*These authors contributed equally to this work.
†Corresponding author. Email: benlev@stanford.edu

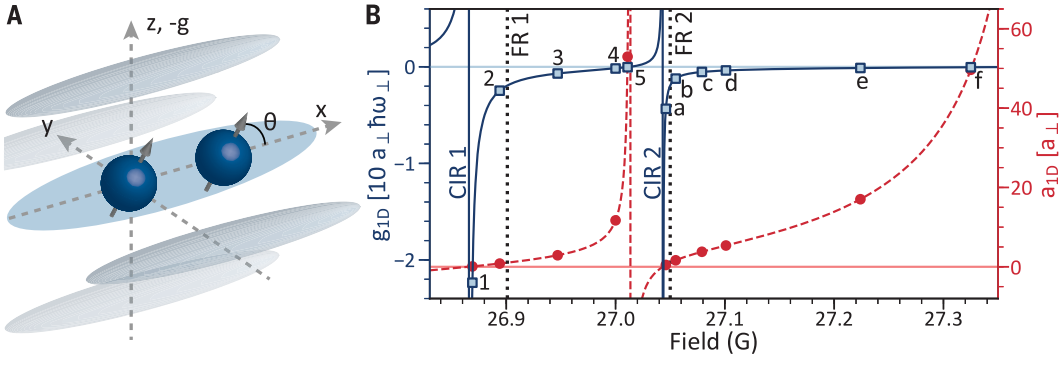

Fig. 1. Experimental concept. (**A**) Atoms are loaded into 1D traps formed by a 2D optical lattice. Atomic dipoles are aligned by a magnetic field at angle θ from $\hat{x}$ in the x–z plane. (**B**) The applied field magnitude tunes the contact interaction strength g_{1D} (solid blue line) and 1D scattering length a_{1D} (dashed red line) via two confinement-induced resonances (CIRs) located on the low-field side of Feshbach resonances (FRs) indicated by black dotted lines. $g_{1D} < 0$ measurements are labeled by numbers and letters for the first and second holonomy cycles, respectively.

Downloaded from http://science.sciencemag.org/ on January 14, 2021

attractive, to create the sTG. As the attractive interactions are tuned away from this unitary contact regime, the sTG gas usually becomes thermodynamically unstable because the bosons can form soliton-like bound cluster states (*15*, *16*, *30*), as has been observed in a nondipolar Cs gas (*18*). By contrast, our dipolar system appears dynamically stable for very long times. This allows us to then ramp the attractive contact interaction strength toward zero again to generate a weakly attractive Bose gas in a highly excited nonthermal state. That the system remains dynamically stable throughout this procedure is a consequence of the repulsive dipolar interactions, as we will discuss below. Repeating the cycle by crossing another CIR produces even higher excited states. These claims are supported through gas stiffness and energy-per-particle measurements at various stages in the protocol.

We begin our experiments by preparing a nearly pure Bose-Einstein condensate (BEC) of highly magnetic Dy atoms at 26.69 G, just shy of the CIRs employed. (^{162}Dy's magnetic moment of $\mu = 10$ Bohr magnetons is 10 times that of, e.g., Cs's, yielding a DDI ~100 times stronger.) After adiabatically rotating the field to a target angle θ with respect to the 1D axis $\hat{x}$, we load the BEC into a 2D optical lattice (*21*) whose first transverse excited-state energy is $\hbar\omega_\perp/k_B = 1180(20)$ nK. The transverse frequency is $\omega_\perp = 2\pi \times 24.6(4)$ kHz; $h = 2\pi\hbar$ is Planck's constant, and k_B is the Boltzmann constant. The lattice comprises an array of ~1000 1D optical traps with about 40 atoms in the central tube and 30 atoms per tube on average; see Fig. 1A and (*22*). Each tube approximates a 1D channel of finite length, where the ratio of longitudinal versus transverse oscillator lengths is $a_\parallel/a_\perp = 25$. The field is then further ramped (in a few milliseconds) to the target magnitude at which collective oscillation measurements are to be performed; see (*22*) for details. These measurements are consistent with zero-temperature ground state predictions (*22*), which implies that the temperature is sufficiently low to observe the sTG gas (*31*).

The system may be described with a Lieb-Liniger (LL) Hamiltonian (*32*, *33*) augmented by the magnetic DDI:

$$H = -\frac{\hbar^2}{2m}\sum_{j=1}^{N}\frac{\partial^2}{\partial x_j^2} + \sum_{1\le i<j\le N}\left[g_{1D}\delta(x_i - x_j) + V_{DDI}^{1D}(\theta, x_i - x_j)\right] \quad (1)$$

where the first two terms comprise the LL model and the third is the 1D-regularized DDI (*22*). Because the DDI scales as $1 - 3\cos^2\theta$, we can control its sign and strength by applying an external magnetic field **B** to polarize the dipoles at any θ. The contact interaction strength g_{1D} is independently controlled by setting the field magnitude B to be near a CIR while holding θ constant; see Fig. 1B.

A CIR appears when the bound state of the first transverse motional excited state of the 1D trap is degenerate with the open-channel transverse ground state. It modifies the contact interaction strength as follows:

$$g_{1D}(B) = -\frac{2\hbar^2}{m a_{1D}(B)} = \frac{2\hbar^2 a_{3D}(B)}{m a_\perp^2}\frac{1}{1 - C a_{3D}(B)/a_\perp} \quad (2)$$

Here, $C \approx 1$ and a_{3D} and a_{1D} are the 3D and 1D scattering lengths, respectively (*24*). We tune g_{1D} by controlling a_{3D} with a Feshbach resonance at fixed $a_\perp$. Feshbach resonances provide a means for tuning a_{3D} through control of B (*34*). The gas enters the unitary contact-interaction regime $\gamma \to \pm\infty$ when B sets $a_{3D} = a_\perp/C$ (*35*). The dimensionless LL parameter is $\gamma = g_{1D}m/\hbar^2 n_{1D}$, with n_{1D} the 1D atomic density.

Although the DDI has been predicted to affect CIRs (*22*, *36*), we resolve no shift of these resonances' positions or widths versus θ in our molecular bound-state measurements (*22*). Indeed, their positions are adequately predicted by the nondipolar theory result of Eq. 2. This simplifies the mapping of B to a_{3D} (and hence to g_{1D}) by rendering it θ-independent. We implement the holonomy cycle(s) by sweeping B up to a desired higher-field value, thereby preparing a state with a particular g_{1D}. The second holonomy cycle begins after point 5 in Fig. 1B, where g_{1D} turns positive again, and continues to point *f* where g_{1D} crosses zero again.

We measure gas stiffness through observations of collective oscillations of the atoms along the 1D trap axis (*18*, *37*, *38*). The frequency ω_B of the breathing mode of the gas is sensitive to its inverse compressibility (stiffness), and thus contains information about correlations. Normalizing ω_B by the frequency ω_D of the center-of-mass dipole (sloshing) mode accounts for nonuniversal aspects of the 1D potentials, such as trap frequencies (*38*). This allows one to compare the stiffness of disparate systems at different interaction strengths by plotting $R = (\omega_B/\omega_D)^2$ versus $A^2 = Na_{1D}^2/a_\parallel^2$. Here, A is the universal form of the coupling constant under the local density approximation (*38*). At strong coupling ($g_{1D} \to \pm\infty$), $A^2 \to 0$, whereas it diverges at weak coupling ($g_{1D} \to 0^\pm$).

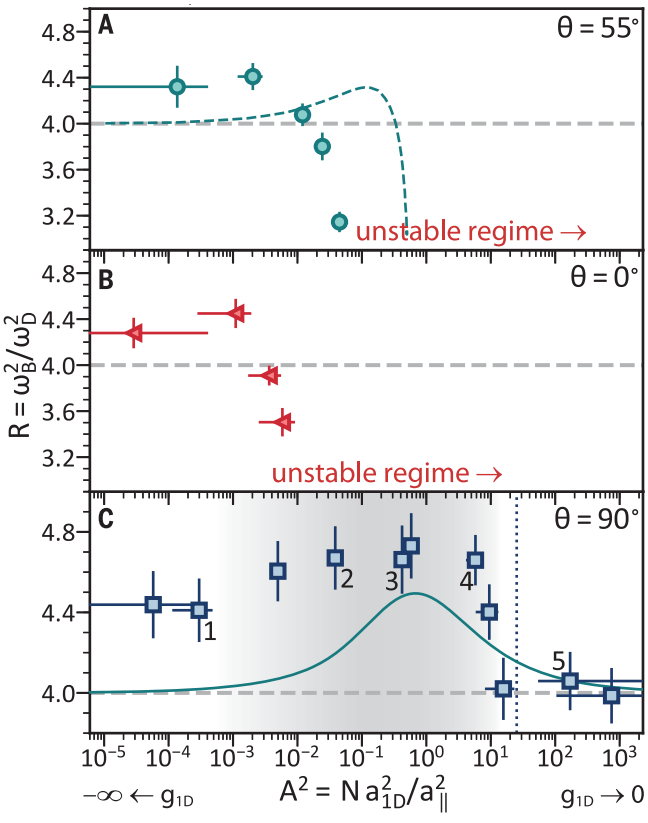

Fig. 2. Post-quench gas stiffness *R* versus interaction parameter A^2. Shown is the attractive $g_{1D} < 0$ regime of the first holonomy cycle for the (**A**) nondipolar ($\theta = 55°$) and (**B**) attractive DDI (0°) system, and for (**C**) the repulsive, 90° DDI-stabilized excited gas. In (A) and (B), an sTG gas exists in the unitary regime of $A^2 \lesssim 10^{-3}$. Beyond, however, the gas softens before collapsing near $A^2 \approx 10^{-1}$ and 10^{-2}, respectively. For comparison, the dashed green curve in (A) plots data from the nondipolar variational Monte Carlo simulation of (*15*). Unexpectedly, the repulsive DDI system in (C) remains stable beyond the unitary regime. This allows correlated prethermal states to emerge around intermediate coupling strengths, indicated by gray shading, before crossing over into the $R = 4$ weakly attractive, excited Bose gas regime beyond $A^2 \approx 10$. The solid curve is the Bethe ansatz prediction of (*18*). The vertical dotted line indicates where the contact and the short-range 1D-regularized DDI contributions become approximately equal (*21*). Numbers refer to points in Figs. 1B and 3. The error bars here and in subsequent figures represent the standard error.

Downloaded from http://science.sciencemag.org/ on January 14, 2021

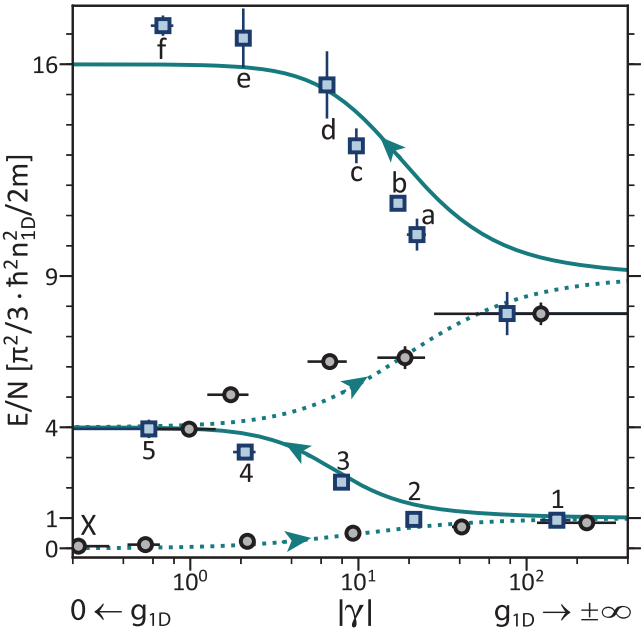

Fig. 3. Energy eigenstate spectrum across two complete quantum holonomy cycles. Shown is the energy per particle E/N for $\theta = 90°$. Black circles (blue squares) are data taken for positive (negative) g_{1D}'s of the repulsive (attractive) LL model. Likewise, dotted (solid) curves are solutions to the Bethe ansatz equations for the repulsive (attractive) nondipolar LL model. In the $g_{1D} \to 0$ and $\pm\infty$ limits, these solutions equal integer multiples of 1/3 times the Fermi energy $\hbar^2(\pi n_{1D})^2/2m$. Arrowheads indicate direction of cycles. The first cycle begins at the point labeled "*X*" and continues to point 5, where the second cycle begins and continues to *f*. The system passes through $|\gamma| \to \infty$ twice as the field increases first through CIR 1, then CIR 2.

To measure oscillations, we selectively excite one of these two modes and hold the gas for a variable amount of time before releasing to image its width or center-of-mass in time-of-flight absorption imaging. We repeat for the other mode and fit the oscillations to extract collective-mode frequencies and R values (*22*).

Figure 2 shows stiffness data for excited states of the attractive ($g_{1D} < 0$) dipolar LL model at three different θ. [Data for ground states of the repulsive $g_{1D} > 0$ model are in (*22*).] We begin with the nondipolar case of $\theta = 55°$ (at which the DDI vanishes along the 1D tube) in Fig. 1A, so as to compare to prior nondipolar Cs measurements (*18*) and to nondipolar theory (*16*). After preparing a TG gas (for which $R = 4$) by tuning $\gamma \to +\infty$ (*22*), we quench into the attractive contact regime where $\gamma \to -\infty, A^2 \to 0$, and the TG gas crosses over into the sTG gas. Tuning A^2 larger causes the stiffness to rise above $R = 4$, indicating that a stiffer—more strongly (anti)correlated—sTG gas forms. At still larger A^2, R rapidly decreases as the gas softens, indicating an imminent collapse into bound cluster states. This trend resembles that reported for the Cs system (*18*), though the exact point of collapse differs from that exhibited in the Cs system. It also differs from the collapse point in the simplified nondipolar variational Monte Carlo calculation of (*15*) (shown as a dashed curve); see (*22*) for discussion. We additionally report metastable states just below $R = 4$: These might be gas-like states of clusters of two or three bound atoms (*17*).

Why should this nondipolar gas collapse, given that the attractive LL model remains integrable for all A^2? In the strictly integrable limit, collapse does not occur, and instead the stiffness rises above $R = 4$ until $A^2 \approx 1$, then decreases to 4 in the weakly attractive regime (*19*). Many-body states with and without clusters belong to separate sectors of Hilbert space, and do not mix. However, in realistic experiments [including nondipolar ones (*18*)], imperfections such as the transverse and longitudinal trap potentials break integrability (*39*–*41*) and yield matrix elements (proportional to the wave function overlap) between the sTG state and the bound cluster states, leading to collapse. In the strongly interacting unitary limit $A^2 \lesssim 10^{-3}$, antibunching strongly suppresses wave function overlap, so the model remains nearly integrable and stable despite experimental imperfections. However, in the intermediate interaction regime, cluster states form and the nondipolar gas is dynamically unstable, as seen in Fig. 2A.

The collapse ensues even earlier if an attractive DDI is introduced by rotating to $\theta = 0°$: Figure 2B shows a collapse beginning at roughly an order-of-magnitude lower in A^2. Evidently, the attractive DDI acts to break integrability at a point deeper within the unitary regime. Indeed, previous work using this experimental platform showed that DDIs generically break integrability (*21*), with equilibration lifetimes that are shortest at 90°. From this perspective, one might also expect an early collapse under a repulsive DDI. Unexpectedly, however, this is not the case: The $\theta = 90°$ data in Fig. 2C show that the sTG remains stable orders of magnitude beyond both that of the nondipolar gas and the 0° attractive DDI gas. Indeed, the repulsive gas never collapses: $R \gtrsim 4$ throughout the pumping sequence, regardless of contact strength in the first holonomy cycle. This includes the regime of vanishing contact interactions wherein nondipolar sTG gases collapse. By contrast, dipolar BECs in higher dimensions collapse whenever the attractive contact exceeds the DDI (*42*), and thus cannot be stably tuned through the regime of intermediate contact interactions.

How the repulsive DDI inhibits the sTG eigenstate from mixing with cluster eigenstates is unclear. Variational Monte Carlo simulations of a nondipolar gas in a harmonic trap may provide some intuition. Such calculations exhibit an energy barrier to collapse that shrinks as A^2 grows (*15*), and the repulsive (attractive) DDI may serve to raise (lower) this barrier. However, given the relatively low DDI energy scale, a more appropriate physical picture may be the following: The attractive and repulsive DDIs induce opposite first-order corrections to the wave function (leading to bunching in one case and antibunching in the other), which respectively enhance or suppress the effects of other integrability-breaking terms. Indeed, the low DDI energy scale does not seem to change the Thomas–Fermi–to–TG crossover of the ground states of the repulsive LL model (*22*). Nevertheless, the DDI does have a pronounced affect on the stability of the excited states, rendering their R dependence quite similar to that predicted by the Bethe ansatz equations (*19*). Quantitative discrepancies are not surprising, as the Bethe ansatz solutions exclude effects caused by, e.g., the DDI, trap, and imperfect state preparation.

Next, we explore those states obtained by sweeping B past the second CIR, thereby entering the second holonomy cycle in g_{1D} as reflected in the eigenenergy spectrum (*13*). Energy per particle E/N is measured in time-of-fight absorption imaging. The average momentum is determined from the expansion time and gas width, ensemble averaged over the 1D trap array (*22*). This is shown in Fig. 3, where E/N is plotted versus γ along with the eigenenergy bands derived from the Bethe ansatz equations (*13*, *19*, *22*). We see that crossing the second CIR maps the system to higher-energy eigenstates than those at the same g_{1D} in the previous topological pumping cycle. The orientation of the quench cycle is crucial: Reversing the sense of the cycle does not implement the topological pump, but leads to collapse (*13*, *22*). The measured energies are in good agreement with the Bethe ansatz predictions.

In the regime between the unitary and weakly interacting regimes—i.e., for $10^{-3} < A^2 < 10$ ($1 < \gamma < 10^2$)—the states that we generate form a hierarchy of long-lived, highly excited states that exhibit persistent athermal behavior. (In this respect, they resemble quantum

Downloaded from http://science.sciencemag.org/ on January 14, 2021

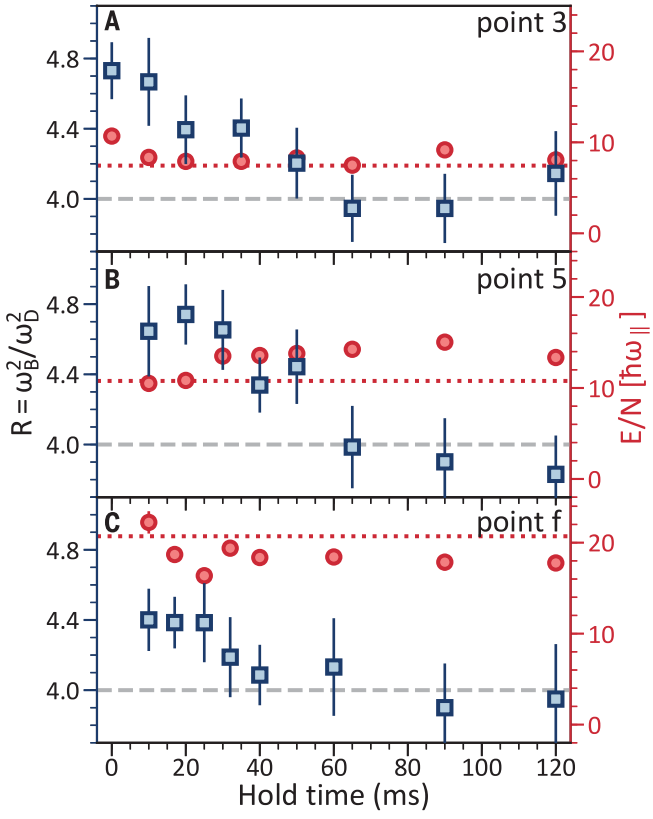

Fig. 4. Evidence for slow thermalization without heating. Plotted are stiffness R (squares) and energy per particle $\frac{E}{N}$ (circles) versus hold time for excited-state gases prepared in the attractive first and second holonomy levels. For reference, $\omega_\parallel = \omega_D$ is $2\pi \cdot 38$–43 Hz for these data and $\theta = 90°$. The time scale associated with the value of ω_B at $t = 0$ in these data is 11 to 12 ms, indicating that the states persist over many oscillation periods. The error bars for the energy per particle data are of the same size or smaller than the data markers. (**A**) Data for the state at point 3. (**B**) and (**C**) show similar data for weakly attractive excited states at points 5 and *f*, respectively. These data are taken by sweeping the field up to the point 5 or *f*, holding, and then sweeping back down to point 3 before making measurements of E/N and R; see text for details. The energy stays approximately constant near the Bethe ansatz prediction (red dotted line) in all cases. This implies that the decay in stiffness toward the thermal-state value $R = 4$ is caused purely by thermalization and is not due to heating (i.e., to an increase in entropy rather than energy). Thus, atypical excited states can be prepared and persist for long times in both the strongly and weakly interacting regimes. Data for points 5 and *f* at $t = 0$ are absent, as these points simply possess the R of the state at point 3.

many-body scars.) To establish this, we demonstrate that they are atypical and distinct from thermal states at the same E/N. We do so by observing both R and the energy of these states as a function of time held in that state. We begin with point 3. Figure 4A shows that although R slowly decreases to the $R = 4$ value of a thermal state (*43*), its E/N stays the same. Thus, in becoming a thermal state, the gas must be increasing its entropy because it does not heat. This implies that the initial strongly correlated state with $R = 4.7$ is atypical, yet sufficiently long-lived to be well-characterized by collective oscillation measurements.

To show that the gas is nonthermal throughout the holonomy cycles, we repeat this measurement for two weakly interacting excited states: points 5 and *f* in the first and second attractive holonomy levels; see Fig. 4, B and C, respectively. Bethe ansatz predicts that these states will have R's close to 4 [as confirmed in (*22*)], inconveniently just like thermal states. To distinguish them from thermal states using stiffness, we sweep B back to point 3 after a variable hold time. Point 3's stiffness is naturally above 4; thus, this method for measuring R should yield values greater than 4 as long as the excited state held at point 5 or *f* is nonthermal. Recall that R is a proxy for anticorrelations in the sTG state. As shown in Fig. 4, B and C, we indeed find that neither gas immediately relaxes to an $R = 4$ thermal state nor significantly heats.

In conclusion, we experimentally realized a spectral topological pump that takes a Bose gas from its ground state to a "ladder" of nonthermal excited states; we demonstrated the first two steps on this ladder. The central topological feature of this pump—quantum holonomy—is only strictly well-defined in the integrable limit. The imperfections in any realistic experiment imply that one is never at the integrable limit, and render the system unstable. However, dipolar interactions (which themselves break integrability) stabilize the sTG against the effects of other integrability-breaking perturbations and increase the lifetime of the prethermal states long enough that one can complete a full cycle and thus experimentally utilize the holonomy. The observation that two integrability-breaking perturbations can counteract each other might have wide-ranging implications for understanding the onset of chaos in nearly integrable quantum systems (*21*, *44*, *45*, *46*). Future work can characterize these excited states through measurements of dynamic susceptibility and lifetime versus θ.

REFERENCES AND NOTES

1. L. D'Alessio, Y. Kafri, A. Polkovnikov, M. Rigol, *Adv. Phys.* **65**, 239–362 (2016).
2. M. Rigol, V. Dunjko, M. Olshanii, *Nature* **452**, 854–858 (2008).
3. R. Vasseur, J. E. Moore, *J. Stat. Mech.* **2016**, 064010 (2016).
4. D. A. Abanin, E. Altman, I. Bloch, M. Serbyn, *Rev. Mod. Phys.* **91**, 021001 (2019).
5. H. Bernien *et al.*, *Nature* **551**, 579–584 (2017).
6. N. Shiraishi, T. Mori, *Phys. Rev. Lett.* **119**, 030601 (2017).
7. C. J. Turner, A. A. Michailidis, D. A. Abanin, M. Serbyn, Z. Papić, *Nat. Phys.* **14**, 745–749 (2018).
8. E. J. Heller, *Phys. Rev. Lett.* **53**, 1515–1518 (1984).
9. S. Moudgalya, S. Rachel, B. A. Bernevig, N. Regnault, *Phys. Rev. B* **98**, 235155 (2018).
10. F. Marcus Kollar, A. Wolf, M. Eckstein, *Phys. Rev. B* **84**, 054304 (2011).
11. V. Khemani, C. R. Laumann, A. Chandran, *Phys. Rev. B* **99**, 161101 (2019).
12. D. J. Thouless, *Phys. Rev. B* **27**, 6083–6087 (1983).
13. N. Yonezawa, A. Tanaka, T. Cheon, *Phys. Rev. A* **87**, 062113 (2013).
14. S. Kasumie, M. Miyamoto, A. Tanaka, *Phys. Rev. A* **93**, 042105 (2016).
15. G. E. Astrakharchik, D. Blume, S. Giorgini, B. E. Granger, *Phys. Rev. Lett.* **92**, 030402 (2004).
16. G. E. Astrakharchik, J. Boronat, J. Casulleras, S. Giorgini, *Phys. Rev. Lett.* **95**, 190407 (2005).
17. M. T. Batchelor, M. Bortz, X. W. Guan, N. Oelkers, *J. Stat. Mech. Theory Exp* **2005**, L10001 (2005).
18. E. Haller *et al.*, *Science* **325**, 1224–1227 (2009).
19. S. Chen, L. Guan, X. Yin, Y. Hao, X.-W. Guan, *Phys. Rev. A* **81**, 031609 (2010).
20. P. Solano *et al.*, *Phys. Rev. Lett.* **123**, 173401 (2019).
21. Y. Tang *et al.*, *Phys. Rev. X* **8**, 021030 (2018).
22. See supplementary materials.
23. M. Olshanii, *Phys. Rev. Lett.* **81**, 938–941 (1998).
24. T. Bergeman, M. G. Moore, M. Olshanii, *Phys. Rev. Lett.* **91**, 163201 (2003).
25. H. Moritz, T. Stöferle, K. Günter, M. Köhl, T. Esslinger, *Phys. Rev. Lett.* **94**, 210401 (2005).
26. E. Haller *et al.*, *Phys. Rev. Lett.* **104**, 153203 (2010).
27. M. Girardeau, *J. Math. Phys.* **1**, 516–523 (1960).
28. B. Paredes *et al.*, *Nature* **429**, 277–281 (2004).
29. T. Kinoshita, T. Wenger, D. S. Weiss, *Science* **305**, 1125–1128 (2004).
30. J. B. McGuire, *J. Math. Phys.* **5**, 622–636 (1964).
31. M. Kormos, G. Mussardo, A. Trombettoni, *Phys. Rev. A* **83**, 013617 (2011).
32. T. Giamarchi, *Quantum Physics in One Dimension*, International Series of Monographs on Physics (Clarendon, 2003).
33. M. A. Cazalilla, R. Citro, T. Giamarchi, E. Orignac, M. Rigol, *Rev. Mod. Phys.* **83**, 1405–1466 (2011).
34. C. Chin, R. Grimm, P. Julienne, E. Tiesinga, *Rev. Mod. Phys.* **82**, 1225–1286 (2010).
35. G. De Rosi, G. E. Astrakharchik, S. Stringari, *Phys. Rev. A* **96**, 013613 (2017).
36. S. Sinha, L. Santos, *Phys. Rev. Lett.* **99**, 140406 (2007).
37. C. Menotti, S. Stringari, *Phys. Rev. A* **66**, 043610 (2002).
38. G. E. Astrakharchik, *Phys. Rev. A* **72**, 063620 (2005).
39. I. E. Mazets, J. Schmiedmayer, *New J. Phys.* **12**, 055023 (2010).
40. S. Tan, M. Pustilnik, L. I. Glazman, *Phys. Rev. Lett.* **105**, 090404 (2010).
41. I. E. Mazets, *Eur. Phys. J. D* **65**, 43–47 (2011).
42. T. Lahaye, C. Menotti, L. Santos, M. Lewenstein, T. Pfau, *Rep. Prog. Phys.* **72**, 126401 (2009).
43. H. Moritz, T. Stöferle, M. Köhl, T. Esslinger, *Phys. Rev. Lett.* **91**, 250402 (2003).
44. B. Bertini, F. H. L. Essler, S. Groha, N. J. Robinson, *Phys. Rev. Lett.* **115**, 180601 (2015).

Downloaded from http://science.sciencemag.org/ on January 14, 2021

45. K. Mallayya, M. Rigol, W. De Roeck, . *Phys. Rev. X* **9**, 021027 (2019).
46. A. J. Friedman, S. Gopalakrishnan, R. Vasseur, *Phys. Rev. B* **101**, 180302 (2020).
47. W. Kao, K.-Y. Li, K.-Y. Lin, S. Gopalakrishnan, B. L. Lev, *Harvard Dataverse* (2020). https://doi.org/10.7910/DVN/H8LX1V.

ACKNOWLEDGMENTS

We thank V. Khemani, G. Astrakharchik, E. Demler, D. Weiss, C. Chin, J. Bohn, D. Petrov, M.-L. Chiofalo, R. Citro, and S. De Palo for stimulating discussions. **Funding:** We acknowledge funding support from AFOSR FA9550-17-1-0266, NSF PHY-2006149, and NSF DMR-1653271. W.K. and K.-Y.Lin acknowledge partial support from NSERC and the Olympiad Scholarship from the Taiwan Ministry of Education, respectively. **Author contributions:** W.K., K.-Y.Li., K.-Y.Lin, and B.L.L. carried out the experiments, and B.L.L. oversaw the work. All authors were involved in the analysis of the results and contributed to writing the paper. **Competing interests:** The authors declare no competing interests. **Data and materials availability:** All experimental data in figures are archived (*47*).

SUPPLEMENTARY MATERIALS

science.sciencemag.org/content/371/6526/296/suppl/DC1
Materials and Methods
Supplementary Text
Figs. S1 to S8
Table S1
References (*48*–*86*)

27 February 2020; accepted 4 December 2020
10.1126/science.abb4928

Downloaded from http://science.sciencemag.org/ on January 14, 2021

Science

Topological pumping of a 1D dipolar gas into strongly correlated prethermal states

Wil Kao, Kuan-Yu Li, Kuan-Yu Lin, Sarang Gopalakrishnan and Benjamin L. Lev

Science **371** (6526), 296-300.
DOI: 10.1126/science.abb4928

Making a quantum pump

Most nonequilibrium, many-particle systems eventually reach a thermal state. However, some one-dimensional quantum systems do not thermalize, although they may settle into a long-term equilibrium state. Kao *et al.* studied such a system consisting of dipolar dysprosium atoms confined in an optical potential shaped like a two-dimensional array of elongated tubes. The authors cycled the contact interaction between the atoms in a prescribed way, creating increasingly excited nonthermal quantum many-body states.

Science, this issue p. 296

ARTICLE TOOLS http://science.sciencemag.org/content/371/6526/296

SUPPLEMENTARY MATERIALS http://science.sciencemag.org/content/suppl/2021/01/13/371.6526.296.DC1

REFERENCES This article cites 85 articles, 2 of which you can access for free
http://science.sciencemag.org/content/371/6526/296#BIBL

PERMISSIONS http://www.sciencemag.org/help/reprints-and-permissions

Use of this article is subject to the Terms of Service

Science (print ISSN 0036-8075; online ISSN 1095-9203) is published by the American Association for the Advancement of Science, 1200 New York Avenue NW, Washington, DC 20005. The title *Science* is a registered trademark of AAAS.

Copyright © 2021 The Authors, some rights reserved; exclusive licensee American Association for the Advancement of Science. No claim to original U.S. Government Works

Downloaded from http://science.sciencemag.org/ on January 14, 2021